HHS Public Access

Author manuscript

Amyloid. Author manuscript; available in PMC 2017 March 01.

Published in final edited form as:

Amyloid. 2016 March ; 23(1): 8–16. doi:10.3109/13506129.2015.1112782.

The pattern recognition reagents RAGE VC1 and peptide p5 share common binding sites and exhibit specific reactivity with AA amyloid in mice

Stephen J. Kennel[1,2], **Angela Williams**[1], **Alan Stuckey**[2], **Tina Richey**[1], **Craig Wooliver**[1], **Walter Chazin**[3], **David A. Stern**[4], **Emily B. Martin**[1], and **Jonathan S. Wall**[1,2]

[1]Department of Medicine, University of Tennessee, Graduate School of Medicine, Knoxville, TN, USA

[2]Department of Radiology, University of Tennessee, Graduate School of Medicine, Knoxville, TN, USA

[3]Departments of Biochemistry and Chemistry, Center for Structural Biology, Vanderbilt University, Nashville, TN, USA

[4]Department of Medicine, University of Tennessee School of Medicine, Memphis, TN, USA

Abstract

In the US, there remains a need to develop a clinical method for imaging amyloid load in patients with systemic, visceral amyloidosis. The receptor for advanced glycation end products (RAGE), which exists as a transmembrane receptor and soluble variant, is found associated with a number of amyloid deposits in man. It is unclear whether amyloid-associated RAGE is the membrane or soluble form; however, given the affinity of RAGE for amyloid, we have examined the ability of soluble RAGE VC1 to specifically localize with systemic AA amyloid in mice. We further compared the reactivity of RAGE VC1 with that of the synthetic, amyloid-reactive peptide p5.

Methods—Binding of radiolabeled RAGE VC1 and p5 to synthetic amyloid fibrils was evaluated using *in vitro* "pulldown" assays in the presence or absence of RAGE ligands. Radioiodinated RAGE VC1 and technetium-99 m-labeled p5 were studied in mice with systemic AA amyloidosis using dual-energy SPECT/CT imaging, biodistribution and microautoradiography.

Results—Soluble RAGE VC1 competed with radioiodinated peptide p5 for binding to rVλ6Wil, Aβ (1–40) and IAPP fibrils but not with the higher affinity peptide, p5R. Pre-incubation with AGE-BSA abrogated binding of VC1 and p5 to rVλ6Wil fibrils. Dual-energy SPECT/CT images and quantitative tissue biodistribution data showed that soluble RAGE VC1 specifically bound AA

Address for correspondence: Jonathan S. Wall, University of Tennessee Medical Center, 1924 Alcoa Highway, Knoxville, TN 37920, USA. Tel: +1 (865) 305 5447. jwall@utmck.edu.

Declaration of interest

This study was supported by PHS grant R01DK079984 to JSW from The National Institute of Diabetes and Digestive and Kidney Diseases (NIDDK) and by PHS grant R01AI101171 to W. J. C. from The National Institute of Allergy and Infectious Disease (NIAID). Additional support was given by the Molecular Imaging and Translational Research Program, and Department of Medicine at UTMCK. J. S. W. and S. K. are inventors on a US patent (# 8.808 666) that describes the use of peptide p5 as an imaging agent for amyloidosis. J. S. W., S. J. K., T. R., E. B. M. and A. S. are equal owners of Solex LLC, which sub-licensed rights to intellectual property from the University of Tennessee.

amyloid-laden organs in mice as effectively as peptide p5. Furthermore, microautoradiography confirmed that RAGE VC1 bound specifically to areas of Congo red-positive amyloid in mouse tissues but not in comparable tissues from control WT mice.

Conclusion—Soluble RAGE VC1 and peptide p5 have similar ligand binding properties and specifically localize with visceral AA amyloid deposits in mice.

Keywords

AA amyloid; AGE-BSA; molecular imaging; peptide p5; receptor for advanced glycation end products; SPECT imaging

Introduction

The receptor for advanced glycation end products (RAGE) is an immunoglobulin super gene family member that binds AGEs, S100 proteins, high mobility group box-1 (HMGB1) protein and soluble forms of the β-amyloid peptide [1–4]. These interactions result in signal transduction that controls a number of inflammation-associated biological processes [5]. RAGE activation, stimulated by binding to its ligands, can lead to activation of NFκB resulting in the production of several proinflammatory mediators. The RAGE activation pathway is regulated by two distinct soluble (s) RAGE variants that act as antagonists of the membrane receptor by binding either AGE moieties or the transmembrane receptor and preventing subsequent cell signaling [6–8]. RAGE activity has been demonstrated, in man, to be associated with the pathogenesis or progression of chronic inflammatory disorders including diabetes as well as cancer and Alzheimer's disease (AD) [9–12].

Amyloidosis is a pathologic process resulting from the aggregation of misfolded peptides and proteins into fibrils and their deposition in organs and tissues [13–15]. This process is associated with numerous diseases including Alzheimer's disease, multiple myeloma and chronic inflammation, and it is a major cause of morbidity and mortality in these patients. More than a decade ago, RAGE was found to be associated with sites of systemic amyloid deposition [16]. Thereafter, RAGE was identified immunohistochemically in human inflammation-associated (AA) amyloid deposits and, to a lesser degree, in deposits of immunoglobulin light chain (AL) amyloid, but RAGE was not associated with sites of transthyretin-associated (ATTR) amyloid deposition [17]. The role of RAGE in the pathogenesis of most amyloid diseases remains enigmatic. However, the binding and translocation of Aβ peptide, as well as activation via the transmembrane form of the RAGE, contributes to the development of amyloid pathology in patients with AD [10–12,18]. Small molecule antagonists as well as sRAGE variants have been shown to be beneficial interventions for the progression of AD [19–23].

Recent work by Haupt et al. has shown that the RAGE VC1 (a synthetic form of RAGE comprising the variable and first constant domain only [24], belongs to a growing family of proteins and peptides that specifically bind amyloid and synthetic amyloid fibrils via principally electrostatic interactions [24–30]. This interaction likely involved the variable immunoglobulin-like domain of RAGE VC1, which has been shown to possess a highly basic surface, evidenced in the high-resolution X-ray crystal structure [8].

We have characterized several synthetic polybasic peptides that, similar to sRAGE, bind amyloid fibrils via electrostatic interactions with the goal of developing a novel radiotracer for the detection of visceral amyloid with molecular imaging [28,30–32]. At present, no such capabilities are available for patients in the US. We have developed a panel of structurally related synthetic peptides with a relatively simple heptad repeating primary structure (A-Q-X-A-Q-A-X, where X is arginine or lysine). These peptides exhibit specific binding to anionic polymers with a distinct charge distribution such as amyloid associated-hypersulfated heparan sulfate and fibrils of various types *in vitro* and *in vivo* [28,29,33]. When radiolabeled, these peptides preferentially bind AA amyloid in mice and can be visualized by using SPECT or PET imaging [28,32]. Since RAGE has also shown to be associated with AA amyloid deposits by immunohistochemistry [17], we hypothesized that the RAGE VC1 protein might also be a useful tool for imaging of amyloid *in vivo*. We, therefore, sought to compare the reactivity of soluble RAGE VC1 with peptide p5 with synthetic fibrils in the presence and absence of competitor molecules *in vitro*. Furthermore, we quantitatively assessed the distribution of ^{125}I-labeled RAGE VC1 and ^{99m}Tc-labeled peptide p5 in mice with systemic AA amyl-oidosis by using dual-energy SPECT/CT imaging, tissue radioactivity measurements and microautoradiography. Herein, we show that RAGE VC1 preferentially binds AA amyloid deposits in mice and that peptide p5 and RAGE VC1 share similar binding sites on synthetic amyloid fibrils. Furthermore, peptide p5 was shown to interact with AGE-BSA, a RAGE ligand, which significantly hindered its interaction with synthetic rVλ6Wil amyloid fibrils.

Methods

Peptide/protein reagents

Recombinant human RAGE VC1 and S100B were produced in *E. coli* and purified as described previously [8,34]. Peptide p5, [CGGYS KAQKA QAKQA KQAQK AQKAQ AKQAK Q] and p5R, [GGGYS RAQRA QARQA RQAQR AQRAQ ARQAR Q], human islet amyloid polypeptide (IAPP) and Aβ(1–40) were purchased from Keck Biosciences (New Haven, CT) and further purified by reverse phase HPLC as described previously [30]. The recombinant (r) λ6 variable domain from patient Wil (rVλ6Wil) was produced in *E. coli* using the pET27B expression vector, isolated from the periplasmic space and purified by reverse-phase HPLC [35]. AGE-BSA, prepared by reaction with glycoaldehyde was from EMD Millipore (Billerica, MA) and BSA was purchased from Sigma-Aldrich (St. Louis, MO). Enoxaparin sodium (Lovenox™) was obtained from the University of Tennessee Medical Center Pharmacy.

Radiolabeling

Peptides (10–40 μg) were radioiodinated with ^{125}I (Perkin Elmer, Waltham, MA) using chloramine T (10 μg) and the products purified by gel filtration and shown to be>95% pure by SDS-PAGE followed by phosphorimager analysis as described elsewhere [36]. For SPECT/CT imaging studies, peptide p5 was radiolabeled with ^{99m}Tc from pertechnitate (Cardinal Health, Knoxville, TN), using 100 ng of $SnCl_2$ according to the method of Tran et al. [37]. The ^{99m}Tc-p5 was purified by gel filtration and characterized by SDS-PAGE and phosphorimaging.

In vitro peptide binding: "pull-down" assays

Approximately 5 ng of ^{125}I-p5 (7.3 nM final concentration) or ^{125}I-p5R (6.8 nM) was added to 50 μg of synthetic amyloid fibrils: rVλ6Wil (19.9 μM), Aβ (1–40) (55 μM), or IAPP (61 μM) in 200 μL PBS/0.05% tween 20 in the presence or absence of RAGE VC1 (19.9 μM). The mixture was rotated, end over end, at RT for 1 h. Samples were then centrifuged twice at 16 000 × *g* for 10 min. Supernatants and pellets were separated after each step and the radioactivity in each was measured using a Cobra II gamma counter (Perkin Elmer) with a 1 min acquisition. The percentage of ^{125}I-p5 or ^{125}I-p5R bound to the fibril pellet was determined as follows:

$$\%\,\mathrm{Bound}=\frac{\mathrm{Pellet\ CPM}}{(\mathrm{Pellet\ CPM}+\mathrm{Supernatant\ CPM})}\times 100.$$

Similar pull down binding assays were performed in the presence of soluble competitors, by pre-incubating AGE-BSA, BSA, enoxaparin or S100B (at 100, 4 or 1 μM) with ^{125}I-p5 or ^{125}I-RAGE VC1 at RT for 30 min, before the addition of 50 μg of synthetic rVλ6Wil fibrils. Competition with S100B was assessed in tris-buffered saline (TBS) with 1 mM $CaCl_2$. All other conditions were as described above.

Systemic AA mouse model

Systemic AA amyloidosis was induced in H2-L^d-huIL-6 Tg Balb/c transgenic mice (H2/IL-6 mice) that constitutively express the human interleukin-6 transgene [38,39] by iv injection of 10 μg of purified, splenic AA amyloid (amyloid enhancing factor; AEF) suspended in 100 μL of sterile phosphate-buffered saline (PBS).

SPECT/CT imaging

The binding of RAGE VC1 and peptide p5 was evaluated in H2/IL-6 mice at 4 and 8 weeks post-AEF injection when amyloid load was modest (2+) or extensive (4+), respectively. Non-transgenic, wild-type (WT) littermates served as controls. Dual-energy SPECT/CT imaging was performed using an Inveon multimodality instrument (Siemens Preclinical Solutions, Knoxville, TN) on mice postmortem. Animals were injected, iv in the lateral tail vein, with ^{125}I-RAGE VC1 (~5 μg, ~100 μCi) mixed with ^{99m}Tc-p5 peptide (~5 μg, ~200 μCi) in 200 μL PBS containing 0.1% gelatin as carrier protein. To delineate abdominal organ boundaries in the CT image, mice received 0.5 mL X-ray contrast agent (Omnipaque™ – [N,N-Bis(2,3-dihydroxypropyl)-5-[N-(2,3-dihydroxypropyl)-acetamido]-2,4,6-triiodo-isophthalamide]; GE Healthcare, Princeton, NJ) i.p. immediately prior to euthanasia and imaging. Dual-energy SPECT (^{99m}Tc/^{125}I) and CT data acquisition and processing parameters were essentially as described elsewhere [30]. All animal studies were performed in accordance with protocols approved by the University of Tennessee Institutional Animal Care and Use Committee and in accordance with the guidelines provided by Office of Laboratory Animal Welfare (OLAW) and the Guide for the Care and Use of Laboratory Animals. The University of Tennessee, Graduate School of Medicine is an AAALAC-I-accredited institution.

Biodistribution and microautoradiography

Following SPECT/CT imaging, a necropsy was performed on each mouse, and samples from 11 tissues (heart, lung, liver, spleen, pancreas, stomach, muscle, left and right kidneys, lower and upper intestines), were taken for radioactivity biodistribution analyses or fixed in buffered formalin for microautoradiographic studies. For biodistribution measurement, tissue samples were placed in tared vials and the radioactivity measured using an automated Wizard 3 gamma counter (1480 Wallac Gamma Counter, Perkin Elmer, Waltham, MA) with a dual isotope protocol and a calculated cross-over correction from the high (^{99m}Tc) to low (^{125}I) energy channel of 4.3%. Data were decay-corrected to the time of injection and expressed as % injected dose per gram of tissue (%ID/g).

For microautoradiography, 6 μm-thick sections were cut from formalin-fixed, paraffin-embedded tissues. The sections were placed on Plus microscope slides (Fisher Scientific, Hampton, NH), dipped in NTB-2 emulsion (Eastman Kodak, Rochester, NY), stored in the dark and developed after a 4-day exposure. Each section was counterstained with hematoxylin and eosin. Detection of amyloid was achieved in consecutive tissue sections by staining with an alkaline Congo red solution (0.8% w/v Congo red, 0.2% w/v KOH, 80% ethanol) for 1 h at room temperature followed by counterstain with Mayer's hematoxylin for 2 min. Note that only the distribution of ^{125}I-RAGE VC1 could be seen in the microautoradiographs since the shorter lived isotope had decayed before exposure to emulsion. All tissue sections were examined using a Leica DM500 light microscope fitted with polarizing filters (for Congo red). Digital microscopic images were acquired using a cooled CCD camera (SPOT; Diagnostic Instruments, Sterling Heights, MI).

Results

Competition of RAGE VC1 for peptide binding to amyloid fibrils

We have developed a semi-quantitative method to study the binding of radiolabeled peptides to synthetic amyloid fibrils. This "pull-down" assay utilized fibrils formed *in vitro* from pure monomer preparations and tested binding of very low concentrations of radiolabeled peptides with a relatively high concentration of target fibrils. We measured, in duplicate, the binding of peptide ^{125}I-p5 and the higher affinity variant, ^{125}I-p5R, to synthetic amyloid fibril preparations composed of rVλ6Wil, Aβ(1–40) or IAPP and competitive inhibition in the presence of RAGE VC1 was assessed (Figure 1). Both peptides bound all three fibril preparations (>50% bound); however, the reactivity of ^{125}I-p5R was greater to IAPP fibrils, likely due to the enhanced affinity. In the presence of RAGE VC1 (at ~2800 molar excess as compared to the peptide), there was a significant reduction in the reactivity of ^{125}I-p5 with all three fibrils types, which was most evident with IAPP fibrils where binding of ^{125}I-p5 was reduced by ~90% (Figure 1A). In contrast, the presence of RAGE VC1 did not cause a reduction in binding of ^{125}I-p5R to rVλ6Wil or Aβ (1–40) fibrils but resulted in an ~70% reduction in binding to IAPP fibrils (Figure 1B).

Given that RAGE VC1 and peptide p5 competed for similar binding sites on amyloid fibrils, we next assessed whether p5 bound RAGE-associated ligands using a competition binding assay (Table 1). Pre-incubation of ^{125}I-RAGE VC1 and p5 with AGE-BSA at 100 μM, but

not 4 μM, significantly reduced the reactivity of these proteins with rVλ6Wil fibrils by ~70 and ~90% for RAGE VC1 and p5, respectively. In contrast, the addition of BSA did not hinder the reactivity of RAGE VC1 with fibrils, but did decrease peptide p5 binding by ~30%. High concentrations (100 μM) of the low molecular weight heparin, Enoxaparin, resulted in a modest decrease (6 and 13%) in the binding of RAGE VC1 and p5 with the synthetic amyloid fibrils. The addition of human recombinant S100B, in the presence of 1 mM $CaCl_2$, had no effect on ^{125}I-RAGE VC1 binding to fibrils but decreased p5 reactivity by 20%, which was similar to the decrease when in the presence of 1 mM $CaCl_2$ alone (Table 1).

Biodistribution of ^{125}I-RAGE VC1 and ^{99m}Tc-p5 in WT mice

Dual-energy SPECT/CT imaging was used to compare the amyloid reactivity of ^{125}I RAGE VC1 and ^{99m}Tc-p5 peptide in the same animal thereby circumventing mouse-to-mouse variability in amyloid load. In amyloid-free WT mice that received ^{125}I-RAGE VC1, radioactivity was observed in the thyroid and stomach due to dehalogenation of the unbound protein in the kidney and liver during catabolism. In contrast, ^{99m}Tc-p5, which is less sensitive to loss of the radionuclide during catabolism, was observed in the intestines and kidneys (not visible) due to the hepatobiliary and renal clearance of the peptide from the circulation (Figure 2). Cross-over and decay-corrected biodistribution data of these radiotracers in WT mice are shown in Table 2 (n = 6 mice). At 2 h post-injection, there was <2 %ID/g of either radionuclide in any organ of WT mice, consistent with the SPECT/CT imaging data (Figure 2). The ^{125}I-RAGE VC1 was apparently retained more than ^{99m}Tc-p5 in these mice; however, this is due to the fact RAGE VC1 is larger and has a longer circulation time. This anomaly was corrected for by calculating tissue-to-muscle ratios (T:M, Table 2). These data confirmed the lack of retention of either probe in healthy tissues.

Biodistribution of ^{125}I-RAGE VC1 and ^{99m}Tc-p5 in AA mice

The biodistribution of ^{125}I-RAGE VC1 and ^{99m}Tc-p5 was assessed, in triplicate, in mice with systemic visceral AA amyloidosis using SPECT/CT imaging (Figure 3). In contrast to WT mice, ^{125}I-RAGE VC1 was observed predominantly in the liver and spleen of mice with AA amyloidosis (Figure 3A–D). These organs represent the major sites of AA amyloid deposition in this mouse model. Only scant activity, relative to the liver and spleen, was observed in the stomach and thyroid of AA mice (Figure 3B and C).

Dual-energy imaging of ^{125}I-RAGE VC1 and ^{99m}Tc-p5 in the same mouse with AA amyloidosis revealed coincident retention of both radiotracers in the amyloid-laden liver and spleen (Figure 3E and F). Weak retention of ^{99m}TC-p5 in the intestines of the AA mice (Figure 3F) that was not seen in the ^{125}I-RAGE VC1 image may represent hepatobiliary clearance of unbound radiotracer or, alternatively, specific uptake of the peptide by intestinal amyloid which is also prevalent in these animals.

Quantitative analysis of the biodistribution of ^{125}I-RAGE VC1 and ^{99m}Tc-p5 radiotracers from the dual-energy imaging studies in mice with extensive AA (4+) or modest AA (2+) amyloid load are presented in Figure 4. Retention of the two radiotracers (%ID/g; Figure 4A and D) show only minor differences; however, ^{125}I-RAGE VC1 uptake was present at higher

concentrations in liver and spleen, as compared to peptide p5, particularly in animals with lower AA burden (Figure 4D). This may be due to the longer circulation time of ^{125}I-RAGE VC1 allowing greater specific accumulation. With respect to radiotracer development, the "disease:healthy uptake" (AA:WT) and the tissue-to-muscle (T:M) ratios are important functional metrics (Figure 4). In this analysis, ^{99m}Tc-p5 showed better discrimination of AA from WT tissues at 2 h post-injection, as evidenced by the higher ratio in amyloid-laden organs such as the liver, spleen, pancreas and intestines. Data for the kidneys, the site of peptide catabolism, was not used in this comparison because radioactivity associated with clearance of the ^{99m}Tc-p5 peptide in the renal cortex did not dissipate during the course of the study.

Amyloid specific uptake of ^{125}I-RAGE VC1

Imaging and tissue biodistribution techniques provide visual and quantitative measures of radiotracer retention in organs, respectively; however, they cannot provide unequivocal evidence to support the specific binding of ^{125}I-RAGE VC1 with the amyloid deposits in the organ. To address this and demonstrate that ^{125}I-RAGE VC1 localized to the amyloid deposits in the designated organs, we performed microautoradiography of tissue sections (Figure 5). Microautoradiographs (ARG) of the spleen and liver from mice injected with ^{125}I-RAGE VC1 showed black silver grain deposition, indicative of the presence of radiotracer. The radiotracer was observed only at sites of amyloid deposition, as evidenced by the co-localization with Congo red (CR) birefringent material seen in consecutive tissue sections (Figure 5A). The specificity of amyloid binding in multiple tissues was further demonstrated by a lack of uptake of ^{125}I-RAGE VC1 in amyloid free tissues from a WT mouse (Figure 5B). Furthermore, these data demonstrated that the specific uptake of ^{125}I-RAGE VC1 by AA in the renal papilla and pancreas are easily seen by this high resolution detection method but are difficult to image effectively, due to the scant amyloid deposits and the limited resolution of the SPECT imaging system (~1 mm). This analysis also revealed that ^{125}I-RAGE VC1 binding to modest (2+) splenic AA was relatively uniform throughout the perifollicular deposit (Figure 5C). In contrast, in mice with extensive (4+) AA, the distribution of ^{125}I-RAGE VC1 was "focal", and the radiotracer did not penetrate fully into areas of dense amyloid (Figure 5C). This phenomenon has been previously observed for high-affinity, amyloid-binding peptides and was attributed to a binding site barrier effect [30].

Discussion

Visceral amyloidosis is associated with a growing number of devastating diseases, and the development of novel methods for detection and treatment are ongoing challenges. Tissue amyloid is a complex matrix composed of linear, non-branching, protein fibrils, proteoglycans and serum proteins. Interestingly, both the glycosaminoglycans (GAGs) and the fibrils represent well-ordered, linear polymers of repeating, charged, disaccharide or protein subunits, respectively. Both these elements represent unique amyloid bio-markers since naturally occurring, functional, extracellular amyloid fibrils are rare in man [40], and amyloid-associated GAGs are hypersulfated and electrochemically distinct from ubiquitous tissue GAG [29,41–43]. In recent years, a growing number of biological agents have been

described that bind multiple forms of amyloid or synthetic amyloid fibrils via principally electrostatic interactions with the charged fibril and/or GAG polymers. Pan- or multi-amyloid reactivity of this kind has been demonstrated with murine mAbs [27], the camelid mAb B10 [24,25], scFv [26], synthetic heparin-reactive peptides [28,30,32], as well as the pattern recognition receptor, RAGE protein [10,16,17,23,24]. Many of these reagents have been radiolabeled and evaluated in mice for their ability to bind and, thereby, image visceral amyloid deposits [29,32], or they are undergoing clinical trials in AL patients as novel therapeutics (e.g. NEOD001; Clincaltrials.gov #NCT02312206).

The exact conformation of the charged interactions is difficult to determine in large reagents such as antibodies; however, they are more readily defined in RAGE VC1 and peptides. Structural analysis of RAGE VC1 provided important insights into the mechanism underlying the interaction with ligands including fibrils [8]. Both the RAGE V and C1 domains have highly electropositive surfaces which facilitate electrostatic interactions with the numerous structurally diverse ligands bound by RAGE. In support of this mechanism, our competition experiments indicated that RAGE VC1 and the polybasic peptides p5 and p5R bind at similar, if not overlapping, sites on synthetic rVλ6Wil, Aβ(1–40) and IAPP fibrils. We have shown that the binding of peptide p5 is dominated by electrostatic interactions between the lysine side chains and the fibrils [30] and, furthermore, that >6 lysine residues are required for significant binding [44]. Moreover, peptide p5R exhibits a greater propensity for α-helical conformation in solution and has a higher affinity for both heparin and synthetic amyloid fibrils [30,45], which likely accounts for the apparent inability of RAGE VC1 to effectively compete with p5R for fibril binding.

Given that the RAGE VC1 bound synthetic amyloid fibrils in a manner similar to peptide p5, via electrostatic interactions, we tested whether peptide p5 also bound non-polymeric RAGE ligands in a reciprocal fashion. Both RAGE VC1 and p5 binding to rVλ6Wil fibrils was dramatically diminished in the presence of AGE-BSA, formed by the reaction of BSA with glycoaldehyde. This reaction results in a rapid modification of lysine and arginine sidechains, ~80 and 20%, respectively, and consequently an increase in the net electronegativity of the BSA within 2 days of incubation [46]. These data suggest that interaction of RAGE VC1 with AGE-BSA, which involves predominantly the variable domain, sterically hinders the interaction with synthetic fibrils. In contrast, the RAGE VC1-fibril interaction was not hindered by the presence of low molecular weight heparin or Ca^{2+}-S100B. Given that RAGE binds S100B, AGE and heparan sulfate principally via interactions with the basic surfaces across the V domain [7,34,47], our data suggest that RAGE VC1 binding to synthetic amyloid fibrils involves a distinct binding region in the C1 domain that does not overlap with the portion of heparan sulfate binding site in this domain [7,34,47]. Remarkably, our data show RAGE VC1 can accommodate interactions with both fibrils and the low molecular weight heparin and Ca^{2+}-S100B ligands simultaneously. However, we anticipate if the ligand is large enough, as in the case of BSA (i.e. twice the molecular weight of the RAGE VC1), steric hindrance may inhibit the interaction.

Peptide p5 binding to synthetic rVVλ6Wil fibrils was similarly hindered by the presence of 100 μM AGE-BSA, a 5-fold molar excess relative to the rVλ6Wil fibrils; however, when the fibrils were at 5-fold molar excess (i.e. 4 μM AGE-BSA) no competition was observed. The

data suggest that the peptide had a higher affinity for the enhanced electronegative surface of modified BSA [46], than for native BSA, which caused only a relatively modest decrease in fibril binding (Table 1). In addition, these data indicate that in an excess of amyloid, peptide p5 and likely similar derivatives [33], preferentially bind amyloid even in the presence of AGE, further supporting the utility of these peptides as imaging agents in patients with systemic amyloidosis.

One of the major concerns in developing a radiotracer probe for amyloid detection is the possible reaction of the reagent with normal tissue, which would complicate interpretation of the image data. It is clear that sRAGE circulates in normal individuals without significant interactions with normal tissue; however, structural and functional data suggest that sRAGE may form oligomeric complexes with transmem-brane RAGE, where the complex can engage ligand without subsequent signal transduction [8,47]. This process is concentration and pH dependent and is enhanced by the presence of Zn^{2+}. In healthy mice lacking amyloid, there was no evidence of cell-binding of ^{125}I-RAGE VC1. This may be due to the low concentration of RAGE VC1 that was used in this study, ~5 μg injected dose (~0.1 μM in the mouse – assuming a blood volume of 1.8 mL), or the fact that healthy mice may not express significant membrane RAGE. Regardless, this biological function of sRAGE molecules may complicate detection of amyloid in patients where membrane RAGE expression is enhanced (see below). Peptide p5 presents a relatively simple pattern of positive charges, a linear array of eight side chains displayed along one face of an α-helix. In healthy mice, there was no reactivity with proteoglycans or other cell surface receptors [28]. To date, we have not identified a biological function for p5.

In contrast, in mice with systemic AA amyloidosis, ^{125}I-RAGE VC1 accumulated rapidly and specifically in amyloid deposits with similar efficiency as the peptide p5. RAGE mRNA copy number in the spleens of mice developing AA have been shown to increase significantly [17]. Thus, radioiodinated sRAGE VC1 could be accumulating in the AA amyloid due to oligomerization with newly synthesized and expressed membrane RAGE; however, it is also possible that the injected material was interacting directly with the amyloid deposit in the absence of oligomerization. We have previously demonstrated that peptide p5 binds both heparin and synthetic amyloid fibrils, and similarly, sRAGE has been shown to bind heparin [48] as well as fibrils [24]. Given the fact that all amyloid deposits contain, in addition to fibrils, significant concentrations of hypersulfated heparan sulfate proteogly-cans, it is possible that ^{125}I-RAGE VC1 may accumulate in amyloid by virtue of an interaction with amyloid-specific GAG motifs. Due to the high negative charge density on these GAGs, significant electrostatic interactions with amyloid GAGs may not require oligomerization of sRAGE VC1. Alternatively, these interactions may give rise to high-order oligomers of sRAGE within the amyloid. Indeed, hypersul-fated heparin dodecasaccharides have been shown to stabilize hexameric conformers of RAGE VC1, a naturally occurring process that may facilitate signal transduction [47].

This study was undertaken to evaluate the amyloid binding of soluble RAGE VC1 and compare its reactivity with the amyloidophilic, polybasic and peptide p5. Both RAGE VC1 and peptide p5 bound synthetic amyloid fibrils via overlapping sites, as RAGE VC1 binding inhibited fibril-reactivity of p5. In addition, pre-incubation of both RAGE VC1 and p5 with

the negatively charged RAGE ligand, AGE-BSA, significantly abrogated the binding with fibrils. When delivered intravenously, radiolabeled RAGE VC1 and p5 specifically localized with systemic AA amyloid deposits, as evidenced by small animal imaging and microautoradiogra-phy – no evidence of RAGE VC1 binding to healthy cells or tissues was evidenced. With respect to developing novel imaging agents for the detection of visceral amyloid in patients, natural products, such as serum proteins, have the potential advantage of being non-immunogenic and less reactive in normal tissue. In addition, they may be relatively easy to traverse the rigors of regulatory approval. Furthermore, dehalogenation of the radioiodinated RAGE VC1 in the kidneys, during catabolism, permitted specific detection of renal amyloid deposits. We have demonstrated the importance of peptide radiotracer dehalogenation for imaging renal amyloid previously [31]. In this study, we used ^{99m}Tc-labeled peptide p5 to allow dual-energy comparison of the two radiotracers in mice; however, ^{99m}Tc accumulated in the renal cortex during catabolism of p5, thereby preventing accurate detection of renal amyloid in the mice with this radiotracer. To effectively image renal amyloid disease in patients with systemic amyloidosis, a radioiodinated peptide probe, such as ^{124}I- or ^{123}I-labeled peptide p5+14 may be optimal for clinical PET or SPECT applications, respectively [31,33].

In this preliminary evaluation, radiolabeled RAGE VC1 proved to be an efficient amyloid imaging agent, albeit not significantly more efficacious than peptide p5. In terms of clinical utility, the use of RAGE VC1 as an imaging agent may be complicated by the fact that the molecule has a biological function which could reduce imaging efficacy, especially in patients with type 2 diabetes and other inflammatory disorders where membrane RAGE is hyper-expressed and may compete for amyloid binding [4,9,49]. This study also raises the possibility that, in patients with amyloidosis, the negative feedback control of the inflammatory response may be compromised due to a recruitment of sRAGE variants by amyloid deposits, e.g. AA and AIAPP, which are commonly found in patients with chronic inflammation and type 2 diabetes, respectively. Finally, when compared to the synthetic peptide p5, RAGE VC1 did not provide significant advantages as an amyloid imaging agent, which further validates clinical evaluation of the radiolabeled peptide, or a similar variant, for amyloid detection in patients with visceral amyloidosis.

Conclusion

Both RAGE VC1 and peptide p5 bind amyloid fibrils via electrostatic interactions at similar sites. Subsequently, both reagents, when radiolabeled, effectively imaged systemic AA amyloid deposits in mice. This class of reagents may prove valuable for amyloid targeting and detection and provide the basis for novel, efficacious diagnostic and therapeutic agents.

Acknowledgments

We would like to thank Jim Wesley for assistance with all aspects of the tissue processing and microautoradiography.

Abbreviations

AD	Alzheimer's disease
AGE	advanced glycation end products
ARG	microautoradiography
IAPP	islet amyloid polypeptide
RAGE	receptor for advanced glycation end products
RAGE VC1	soluble recombinant variable and constant-1 domains of RAGE
rVλ6	recombinant λ6 light chain variable region
SAA	serum amyloid protein A
SPECT/CT	single photon emission computed/X-ray computed tomography
TTR	transthyretin

References

1. Bierhaus A, Humpert PM, Morcos M, Wendt T, Chavakis T, Arnold B, Stern DM, et al. Understanding RAGE, the receptor for advanced glycation end products. J Mol Med (Berl). 2005; 83:876–86. [PubMed: 16133426]
2. Bucciarelli LG, Wendt T, Rong L, Lalla E, Hofmann MA, Goova MT, Taguchi A, et al. RAGE is a multiligand receptor of the immunoglobulin superfamily: implications for homeostasis and chronic disease. Cell Mol Life Sci. 2002; 59:1117–28. [PubMed: 12222959]
3. Schmidt AM, Yan SD, Yan SF, Stern DM. The biology of the receptor for advanced glycation end products and its ligands. Biochim Biophys Acta. 2000; 1498:99–111. [PubMed: 11108954]
4. Stern D, Yan SD, Yan SF, Schmidt AM. Receptor for advanced glycation endproducts: a multiligand receptor magnifying cell stress in diverse pathologic settings. Adv Drug Deliv Rev. 2002; 54:1615–25. [PubMed: 12453678]
5. Sparvero LJ, Asafu-Adjei D, Kang R, Tang D, Amin N, Im J, Rutledge R, et al. RAGE (Receptor for Advanced Glycation Endproducts), RAGE ligands, and their role in cancer and inflammation. J Transl Med. 2009; 7:17.10.1186/1479-5876-7-17 [PubMed: 19292913]
6. Vazzana N, Santilli F, Cuccurullo C, Davi G. Soluble forms of RAGE in internal medicine. Intern Emerg Med. 2009; 4:389–401. [PubMed: 19727582]
7. Yan SF, Ramasamy R, Schmidt AM. Soluble RAGE: therapy and biomarker in unraveling the RAGE axis in chronic disease and aging. Biochem Pharmacol. 2010; 79:1379–86. [PubMed: 20096667]
8. Koch M, Chitayat S, Dattilo BM, Schiefner A, Diez J, Chazin WJ, Fritz G. Structural basis for ligand recognition and activation of RAGE. Structure. 2010; 18:1342–52. [PubMed: 20947022]
9. Stern DM, Yan SD, Yan SF, Schmidt AM. Receptor for advanced glycation endproducts (RAGE) and the complications of diabetes. Ageing Res Rev. 2002; 1:1–15. [PubMed: 12039445]
10. Arancio O, Zhang HP, Chen X, Lin C, Trinchese F, Puzzo D, Liu S, et al. RAGE potentiates Abeta-induced perturbation of neuronal function in transgenic mice. EMBO J. 2004; 23:4096–105. [PubMed: 15457210]
11. Fang F, Lue LF, Yan S, Xu H, Luddy JS, Chen D, Walker DG, et al. RAGE-dependent signaling in microglia contributes to neuroinflammation, Abeta accumulation, and impaired learning/memory in a mouse model of Alzheimer's disease. FASEB J. 2010; 24:1043–55. [PubMed: 19906677]
12. Yan SS, Chen D, Yan S, Guo L, Du H, Chen JX. RAGE is a key cellular target for Abeta-induced perturbation in Alzheimer's disease. Front Biosci (Schol Ed). 2012; 4:240–50. [PubMed: 22202057]

13. Blancas-Mejia LM, Ramirez-Alvarado M. Systemic amyloidoses. Annu Rev Biochem. 2013; 82:745–74. [PubMed: 23451869]
14. Merlini G, Bellotti V. Molecular mechanisms of amyloidosis. N Engl J Med. 2003; 349:583–96. [PubMed: 12904524]
15. Pepys MB. Amyloidosis. Annu Rev Med. 2006; 57:223–41. [PubMed: 16409147]
16. Yan SD, Zhu H, Zhu A, Golabek A, Du H, Roher A, Yu J, et al. Receptor-dependent cell stress and amyloid accumulation in systemic amyloidosis. Nat Med. 2000; 6:643–51. [PubMed: 10835680]
17. Rocken C, Kientsch-Engel R, Mansfeld S, Stix B, Stubenrauch K, Weigle B, Buhling F, et al. Advanced glycation end products and receptor for advanced glycation end products in AA amyloidosis. Am J Pathol. 2003; 162:1213–20. [PubMed: 12651613]
18. Deane R, Du Yan S, Submamaryan RK, LaRue B, Jovanovic S, Hogg E, Welch D, et al. RAGE mediates amyloid-beta peptide transport across the blood-brain barrier and accumulation in brain. Nat Med. 2003; 9:907–13. [PubMed: 12808450]
19. Sabbagh MN, Agro A, Bell J, Aisen PS, Schweizer E, Galasko D. PF-04494700, an oral inhibitor of receptor for advanced glycation end products (RAGE), in Alzheimer disease. Alzheimer Dis Assoc Disord. 2011; 25:206–12. [PubMed: 21192237]
20. Saito S, Ihara M. New therapeutic approaches for Alzheimer's disease and cerebral amyloid angiopathy. Front Aging Neurosci. 2014; 6:290.10.3389/fnagi.2014.00290 [PubMed: 25368578]
21. Walker D, Lue LF, Paul G, Patel A, Sabbagh MN. Receptor for advanced glycation endproduct modulators: a new therapeutic target in Alzheimer's disease. Expert Opin Investig Drugs. 2015; 24:393–9.
22. Lee YS, Kim H, Kim YH, Roh EJ, Han H, Shin KJ. Synthesis and structure-activity relationships of tri-substituted thiazoles as RAGE antagonists for the treatment of Alzheimer's disease. Bioorg Med Chem Lett. 2012; 22:7555–61. [PubMed: 23140885]
23. Yan SD, Bierhaus A, Nawroth PP, Stern DM. RAGE and Alzheimer's disease: a progression factor for amyloid-beta-induced cellular perturbation? J Alzheimers Dis. 2009; 16:833–43. [PubMed: 19387116]
24. Haupt C, Bereza M, Kumar ST, Kieninger B, Morgado I, Hortschansky P, Fritz G, et al. Pattern recognition with a fibril-specific antibody fragment reveals the surface variability of natural amyloid fibrils. J Mol Biol. 2011; 408:529–40. [PubMed: 21376731]
25. Haupt C, Morgado I, Kumar ST, Parthier C, Bereza M, Hortschansky P, Stubbs MT, et al. Amyloid fibril recognition with the conformational B10 antibody fragment depends on electrostatic interactions. J Mol Biol. 2011; 405:341–8. [PubMed: 21059358]
26. Smits NC, Kurup S, Rops AL, ten Dam GB, Massuger LF, Hafmans T, Turnbull JE, et al. The heparan sulfate motif (GlcNS6S-IdoA2S)3, common in heparin, has a strict topography and is involved in cell behavior and disease. J Biol Chem. 2010; 285:41143–51. [PubMed: 20837479]
27. Wall JS, Kennel SJ, Williams A, Richey T, Stuckey A, Huang Y, Macy S, et al. AL amyloid imaging and therapy with a monoclonal antibody to a cryptic epitope on amyloid fibrils. PLoS One. 2012; 7:e52686. [PubMed: 23300743]
28. Wall JS, Richey T, Stuckey A, Donnell R, Macy S, Martin EB, Williams A, et al. In vivo molecular imaging of peripheral amyloidosis using heparin-binding peptides. Proc Natl Acad Sci USA. 2011; 108:E586–94. [PubMed: 21807994]
29. Wall JS, Richey T, Stuckey A, Donnell R, Oosterhof A, van Kuppevelt TH, Smits NC, et al. SPECT imaging of peripheral amyloid in mice by targeting hyper-sulfated heparan sulfate proteoglycans with specific scFv antibodies. Nucl Med Biol. 2012; 39:65–75. [PubMed: 21958847]
30. Wall JS, Williams A, Richey T, Stuckey A, Huang Y, Wooliver C, Macy S, et al. A binding-site barrier affects imaging efficiency of high affinity amyloid-reactive peptide radiotracers in vivo. PLoS One. 2013; 8:e66181. [PubMed: 23750281]
31. Martin EB, Kennel SJ, Richey T, Wooliver C, Osborne D, Williams A, Stuckey A, et al. Dynamic PET and SPECT imaging with radioiodinated, amyloid-reactive peptide p5 in mice: a positive role for peptide dehalogenation. Peptides. 2014; 60:63–70. [PubMed: 25102446]

32. Wall JS, Richey T, Williams A, Stuckey A, Osborne D, Martin E, Kennel SJ. Comparative analysis of peptide p5 and serum amyloid P component for imaging AA amyloid in mice using dual-isotope SPECT. Mol Imaging Biol. 2012; 14:402–7. [PubMed: 22042488]
33. Wall JS, Martin EB, Richey T, Stuckey AC, Macy S, Wooliver C, Williams A, et al. Preclinical validation of the heparin-reactive peptide p5+14 as a molecular imaging agent for visceral amyloidosis. Molecules. 2015; 20:7657–82. [PubMed: 25923515]
34. Dattilo BM, Fritz G, Leclerc E, Kooi CW, Heizmann CW, Chazin WJ. The extracellular region of the receptor for advanced glycation end products is composed of two independent structural units. Biochemistry. 2007; 46:6957–70. [PubMed: 17508727]
35. Wall J, Schell M, Murphy C, Hrncic R, Stevens FJ, Solomon A. Thermodynamic instability of human lambda 6 light chains: correlation with fibrillogenicity. Biochemistry. 1999; 38:14101–8. [PubMed: 10529258]
36. Wall JS, Paulus MJ, GLeason S, Gregor J, Solomon A, Kennel SJ. Micro-imaging of amyloid in mice. Meth Enzymol. 2006; 412:161–82. [PubMed: 17046658]
37. Tran T, Engfeldt T, Orlova A, Widstrom C, Bruskin A, Tolmachev V, Karlstrom AE. In vivo evaluation of cysteine-based chelators for attachment of 99mTc to tumor-targeting Affibody molecules. Bioconjug Chem. 2007; 18:549–58. [PubMed: 17330952]
38. Solomon A, Weiss DT, Schell M, Hrncic R, Murphy CL, Wall J, McGavin MD, et al. Transgenic mouse model of AA amyloidosis. Am J Pathol. 1999; 154:1267–72. [PubMed: 10233864]
39. Wall JS, Richey T, Allen A, Donnell R, Kennel SJ, Solomon A. Quantitative tomography of early-onset spontaneous AA amyloidosis in interleukin 6 transgenic mice. Comp Med. 2008; 58:542–50. [PubMed: 19149411]
40. Iconomidou VA, Hamodrakas SJ. Natural protective amyloids. Curr Protein Pept Sci. 2008; 9:291–309. [PubMed: 18537684]
41. Lindahl B, Lindahl U. Amyloid-specific heparan sulfate from human liver and spleen. J Biol Chem. 1997; 272:26091–4. [PubMed: 9334172]
42. Stenstad T, Magnus JH, Husby G. Characterization of proteogly-cans associated with mouse splenic AA amyloidosis. Biochem J. 1994; 303:663–70. [PubMed: 7980430]
43. Sugumaran G, Elliott-Bryant R, Phung N, Vitseva O, Kuberan B, Lech M. Characterization of splenic glycosaminoglycans accumulated in vivo in experimentally induced amyloid-susceptible and amyloid-resistant mice. Scand J Immunol. 2004; 60:574–83. [PubMed: 15584968]
44. Wall JS, Solomon A, Kennel SJ. Development and evaluation of agents for targeting visceral amyloid. Tijdschr Nucl Geneeskd. 2011; 33:807–14. [PubMed: 23885194]
45. Rullo A, Nitz M. Importance of the spatial display of charged residues in heparin-peptide interactions. Biopolymers. 2009; 93:290–8. [PubMed: 19885920]
46. Nagai R, Matsumoto K, Ling X, Suzuki H, Araki T, Horiuchi S. Glycolaldehyde, a reactive intermediate for advanced glycation end products, plays an important role in the generation of an active ligand for the macrophage scavenger receptor. Diabetes. 2000; 49:1714–23. [PubMed: 11016456]
47. Xu D, Young JH, Krahn JM, Song D, Corbett KD, Chazin WJ, Pedersen LC, et al. Stable RAGE-heparan sulfate complexes are essential for signal transduction. ACS Chem Biol. 2013; 8:1611–20. [PubMed: 23679870]
48. Liu R, Mori S, Wake H, Zhang J, Liu K, Izushi Y, Takahashi HK, et al. Establishment of in vitro binding assay of high mobility group box-1 and S100A12 to receptor for advanced glycation end-products: heparin's effect on binding. Acta Med Okayama. 2009; 63:203–11. [PubMed: 19727205]
49. Bierhaus A, Stern DM, Nawroth PP. RAGE in inflammation: a new therapeutic target? Curr Opin Investig Drugs. 2006; 7:985–91.

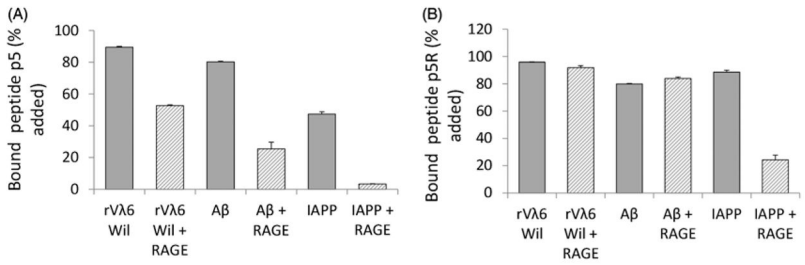

Figure 1.

Binding of RAGE VC1 to synthetic amyloid fibrils involves the same motif as peptide p5. Binding of peptides ^{125}I-p5, 7.3 nM (A) or ^{125}I-p5R, 6.8 nM (B) to synthetic rVλ6Wil (AL), Aβ(1–40) and IAPP fibrils in the absence (dark) or presence (striped) of unlabeled RAGE VC1 in ~2800 molar excess Data presented are mean ± SD of duplicate experiments.

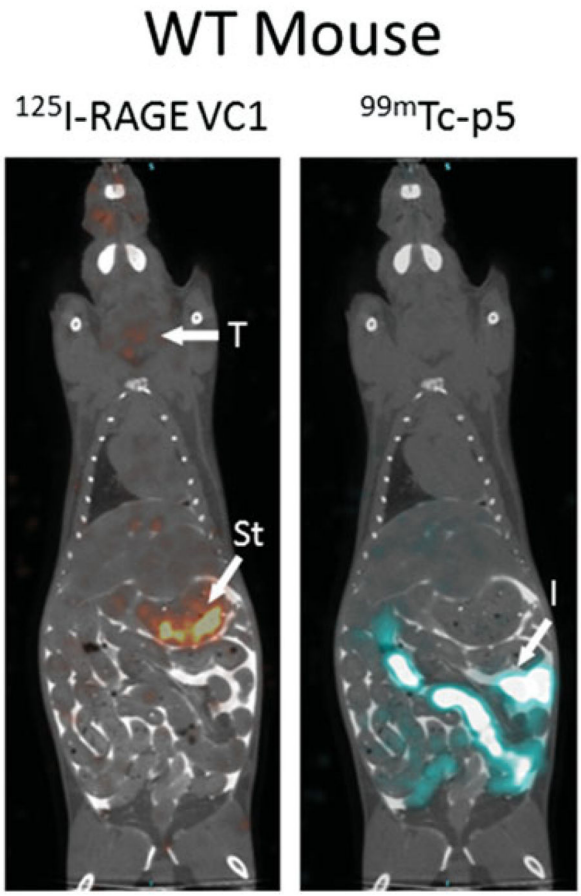

Figure 2.

Dual-energy SPECT/CT imaging of ^{125}I-RAGE VC1 and ^{99m}Tc-p5 in mice. In amyloid-free WT mice there was no specific uptake of either radiotracer in healthy organs. Radioactivity seen in the thyroid (T), stomach (St) and intestines (I) is associated with protein catabolism and hepatobilliary clearance, respectively. In mice with AA amyloidosis, both reagents were observed in the liver (L) and spleen (S), sites of significant amyloid in this mouse model. Imaging was 2 h post-injection iv of 5 μg (100 μCi) of ^{125}I-RAGE VC1 and 5 μg (200 μCi) of ^{99m}Tc-p5.

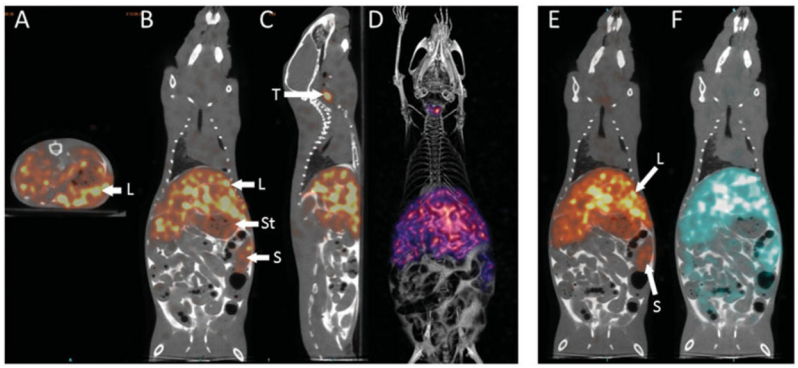

Figure 3.

RAGE VC1 binds preferentially to systemic AA amyloid *in vivo*. Contrast enhanced SPECT/CT imaging at 2 h post-injection of ^{125}I-RAGE VC1 in representative mice with systemic AA (A–D) and dual-energy SPECT/CT images of ^{125}I-RAGE VC1 and ^{99m}Tc-p5 in a representative single mouse with AA (E & F). Radiolabeled ^{125}I-RAGE (red) was observed in amyloid-laden liver (L) and spleen (S) of mice, with free radioiodide in the thyroid (T) and stomach (St). Three-dimensional image views (D) confirmed the hepatosplenic uptake of ^{125}I-RAGE VC1. The distribution of ^{125}I-RAGE VC1 in AA mice was consistent with that of the amyloid-reactive peptide ^{99m}Tc-p5 in AA mice (E–F). Image views: A, axial; B, E and F, coronal; C, sagittal; and D, 3D representation.

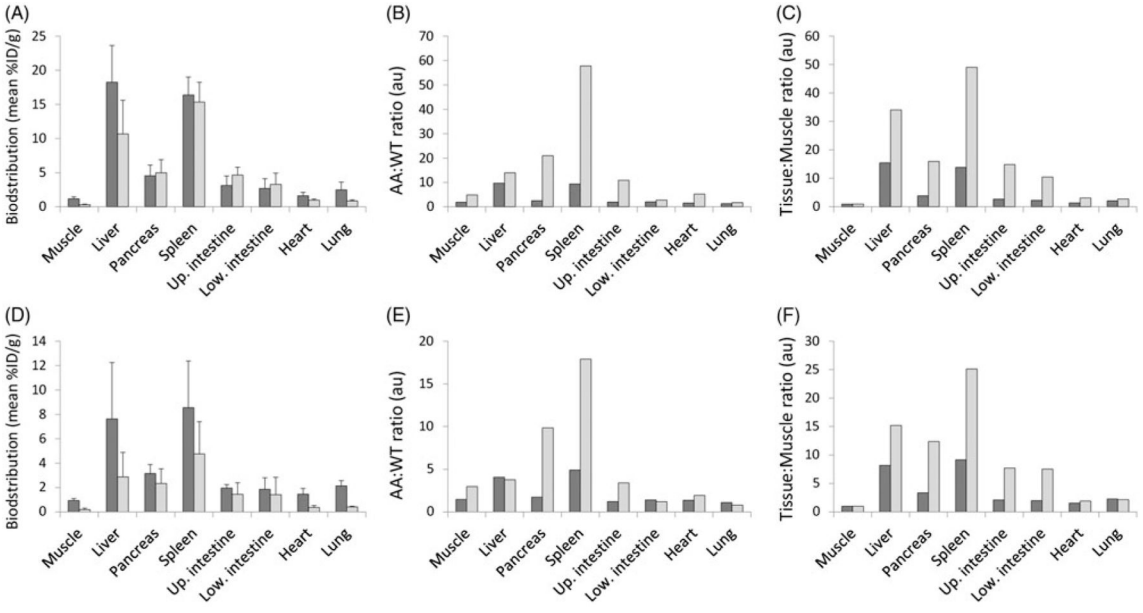

Figure 4.

Reactivity of RAGE VC1 and peptide p5 with AA amyloid-laden tissues *in vivo*. Dual-energy tissue biodistribution measurements, AA-to-WT ratios and tissue-to-muscle ratios of ^{125}I-RAGE VC1 (dark) and ^{99m}Tc-p5 peptide (light) in mice with 4+ (A–C) or 2 + (D–F) systemic AA amyloidosis (mean, $n = 3$). All mice were scored for disease severity using a scale from 0 to 4+ amyloid load, based on Congo red-stained tissue sections).

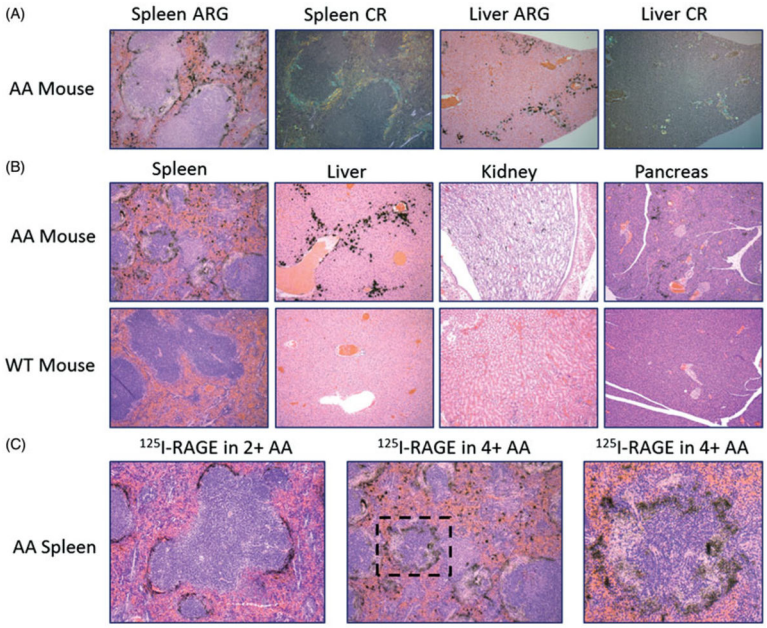

Figure 5.

^{125}I-RAGE VC1 binds preferentially to systemic AA amyloid *in vivo* with high affinity. (A) Analysis of ^{125}I-RAGE VC1 in the spleen and liver of a representative 4+ AA mouse at 2 h post-injection. The distribution of radiolabeled RAGE VC1, evidenced as black silver deposits in the microautoradiographs (ARG), correlated with the deposition of amyloid stained with Congo red (CR) in consecutive tissue sections. (B) ^{125}I-RAGE VC1 deposited in AA amyloid in the mouse spleen, liver, kidney and pancreas but was not observed in tissues from WT mice. (C) ^{125}I-RAGE VC1 effectively infiltrated amyloid in a 2+ AA mouse but not the dense splenic amyloid deposits in a 4+ AA mouse. Boxed area in the middle image is shown magnified in the last panel.

Table 1

Binding of ^{125}I-RAGE VC1 and peptide ^{125}I-p5 to rVλ6 Wil fibrils in the presence of RAGE ligands.

Inhibitors (concentration)	Solution	^{125}I-RAGE VC1 bound*	^{125}I-p5 bound*
No inhibitor	PBS	100.0	100.0
AGE-BSA (100 μM)	PBS	31.1	13.3
AGE-BSA (4 μM)	PBS	99.1	95.5
BSA (100 μM)	PBS	99.8	72.8
BSA (4 μM)	PBS	96.2	96.4
Enoxaparin™ (100 μM)	PBS	94.0	87.4
Enoxaparin™ (4 μM)	PBS	102.5	97.6
No inhibitor	TBS with 1 mM $CaCl_2$	101.7	76.5
S100B (1 μM)	TBS with 1 mM $CaCl_2$	97.2	80.2

*% bound relative to no inhibitor. Measurements represent the mean of duplicate experiments.

Table 2

Biodistribution and tissue to muscle ratios of ^{125}I-RAGE VC1 and ^{99m}Tc-p5 in WT mice.

	^{125}I-RAGE VC1		^{99m}Tc-p5	
	%ID/g (Mean ± SD)	T:M ratio	%ID/g (Mean ± SD)	T:M ratio
Muscle	0.66 ± 0.07	1.00	0.05 ± 0.02	1.00
Liver	1.97 ± 0.17	2.97	0.60 ± 0.19	12.44
Pancreas	1.90 ± 0.21	2.86	0.19 ± 0.07	3.92
Spleen	1.69 ± 0.17	2.55	0.22 ± 0.06	4.65
L. Kidney	3.38 ± 1.43	5.10	31.73 ± 8.77	659.97
R. Kidney	2.67 ± 0.61	4.02	34.22 ± 9.07	711.82
Stomach	7.90 ± 3.18	11.91	0.46 ± 0.33	9.62
Up. Intestine	1.70 ± 0.16	2.57	0.43 ± 0.13	8.88
Low. Intestine	1.28 ± 0.10	1.93	0.70 ± 0.79	14.55
Heart	1.10 ± 0.07	1.66	0.13 ± 0.06	2.75